Data Collection Strategies, Analysis, and Interpretation in AP–XAS

David N. Mueller*

Peter Grünberg Institute, Forschungszentrum Jülich, 52425 Jülich, Germany
***E-mail: dav.mueller@fz-juelich.de**

This chapter will focus on strategies to collect meaningful X-ray absorption data in an ambient medium covering both the hard and soft X-ray regime and how to guide analysis, keeping experimental and physical differences of various strategies in mind. A special interest will be put on how the interaction of primary radiation and signal carriers with the surrounding medium will influence data acquisition and interpretation. Since hard and soft X-rays can be used to probe different electron shells in a material, both experiments can yield important and complementary information. Dipole selection rules lead to vastly different behavior of K- and L-edge XAS of transition metals, for example. In their ambient pressure variants, two major issues (that are fundamentally intertwined) arise when interpreting the data collected from both techniques: Whereas hard X-rays can penetrate condensed matter on a macroscopic scale making true transmission experiments possible, soft X-rays are confined to either electron or fluorescence yield detection modes, the latter suffering from low yields from lighter elements. Those not only pose different experimental challenges to avoid signal loss due to absorption in the reaction medium, but also probe depths of different orders of magnitude.

Preface

In this chapter, we will discuss the implications the presence of a medium surrounding the sample will have on X-ray absorption spectroscopy (XAS) studies. Whereas in the hard X-ray regime (>2 keV photon energy) issues directly related to the "ambient pressure" aspect are much less prevalent and are usually solvable with choice of reactor design, in the soft X-ray regime several compounding effects can lead to severely contaminated spectra. These effects are largely due to the simple fact that both the reaction medium and the solid share the same type of elements, and XAS will probe both indiscriminately. Though this is also the case in ambient pressure X-ray photoelectron spectroscopy, there *e.g.* gas phase and oxide oxygen species are well separated. This is not true for XAS, making interpretation and comparison of samples, especially across different beamlines/experiments, hard, if not impossible. We will discuss the origins of these effects, and present ways to identify and alleviate them in the soft XAS regime. We will also discuss briefly how hard XAS experiments can be designed to further minimize the already much lesser impact there. For completeness, differences in the data obtained from soft and hard ambient pressure (AP)–XAS and their complementary interpretation will be discussed.

Attenuation of the Incident Photons by the Gas Phase

The biggest challenge to overcome in ambient pressure X-ray spectroscopies, especially in the soft X-ray regime, is the small inelastic mean free path (IMFP) of photoelectrons that are detected. This issue has been alleviated by elaborate pumping schemes and sample/detector geometries, minimizing the path the photoelectrons have to travel through the medium (*1*). What should not be neglected, though, is the fact that the incident X-ray photons are also attenuated by matter, albeit to an orders of magnitude lesser extent. Figure 1 shows a comparison of the absorption lengths of photons (solid line) and the inelastic mean free path of electrons (dashed line), both defined as the distance it takes to attenuate the intensity to 1/*e*. The energy E dependent IMFP $\lambda(E)$ was calculated from Seah's universal curve (*2*) as described by

$$\lambda(E) = 0.064\sqrt{E} \tag{1}$$

The IMFP values were scaled to the density of atmospheric pressure from that of a solid by a factor of 1000. It should be noted that this is a rough approximation and only valid for energies $E > 100$ eV, and thus serves as a ballpark estimate, with the focus on the attenuation of photons (*3*).

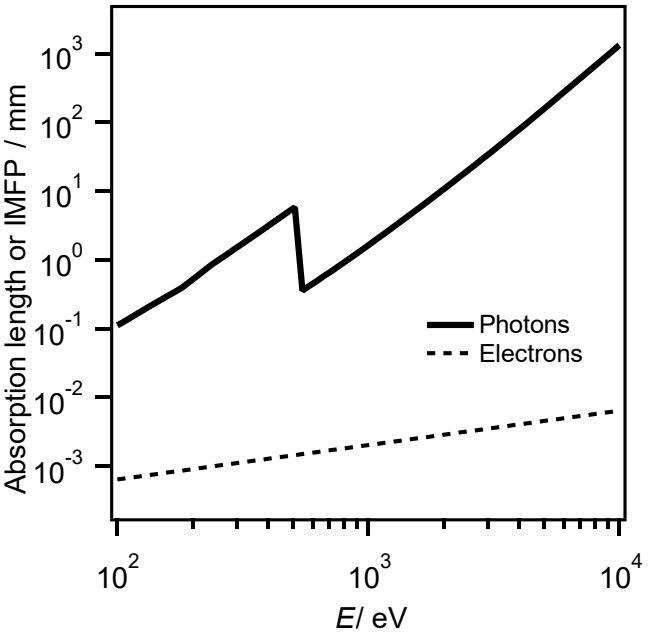

Figure 1. Comparison of the absorption length of photons (solid line) and IMFP of electrons (dotted line) as a function of photon and kinetic energy, respectively, in 1 atm of O_2. Clearly visible in the photon absorption length is the oxygen K-edge at ~530 eV. Calculated using data from ref 3.

Even though the attenuation of the incident photons is two or more orders of magnitude lower than that of the electrons, the absorption lengths adopt values that are to be considered in *in situ* environments, even for the hard X-ray regime. Here, at typical absorption edges of interest, such as the 3d transition metal K-edges (e.g., Fe K-edge at ~7.1 keV), the absorption lengths are on the order of centimeters or tens of centimeters. Even though this issue can be alleviated by the ever-increasing intensity of hard XAS beamlines, it should still be considered in reactor design for in situ studies, as will be discussed later in this chapter.

In the soft X-ray regime, the even greater loss of incident intensity is exacerbated by the presence of absorption edges of the reaction medium itself. In Figure 1, this is made obvious by the kink at ~530 eV, corresponding to the oxygen K-edge. In the (experimentally) worst–but arguably scientifically most interesting–case, the reaction medium and investigated solid share the same elements, making it a challenge to deconvolute both absorption signals. As an example, to showcase this, we turn to the field of solid-state electrochemistry of oxides, where the ubiquitous oxygen exchange reaction

$$\frac{1}{2}O_2 + v_O + 2e^- \rightleftharpoons O^{2-} \qquad (2)$$

(with v_O denoting a vacancy, adopting Norby's notation [*4*]) takes place at the solid–gas interface at elevated temperature (*5*), the equilibrium being driven by either electrical (changing the concentration of electrons) or chemical means (changing the oxygen partial pressure). In the late 3d transition metal (TM) mixed conducting oxides most used as catalysts in this field (*6,7*) strong hybridization of the TM3d and O2p orbitals occurs (*8*), and thus oxidation and reduction are best observed and quantified at the oxygen K-edge (*9–12*). That the use of varying oxygen gas pressure in the XAS chamber can cause distortions in the spectra can be observed on the $Sr(Ti,Co)O_{3-\delta}$ (STC) material, where the use of low Co concentrations breaks the Co3d–O2p hybridization, causing the O-K-edge to be silent upon reduction and oxidation (*13*).

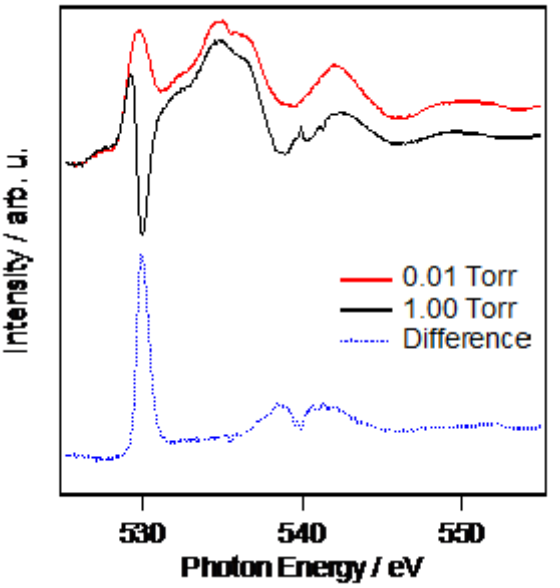

Figure 2. O-K-edge spectra of $Sr(Ti,Co)O_{3-\delta}$ recorded at 500 °C in 0.01 (red solid line) and 1 Torr (black solid line) of oxygen atmosphere in partial electron yield mode. Spectra were background corrected by subtracting the pre-edge intensity at 525 eV. Offset on the intensity axis is the difference of reducing to oxidizing atmosphere, showing the π^* (~530 eV) and σ^* (~540 eV) resonances of the O_2 molecule.

Figure 2 shows oxygen K-edge X-ray absorption spectra recorded at beamline 9.3.1, advanced light source (ALS), Berkeley at 500 °C and varying oxygen partial pressure. Red and black solid lines show the *non-normalized* (just background corrected) spectra at 0.01 and 1 Torr of O_2, respectively, in partial electron yield mode. At a first glance, the spectra look quite different, which could lead to the false interpretation of the electronic structure changing significantly with respect to changes in the oxygen partial pressure. Looking at the leading edges at ~528 eV, which would show any changes in the occupancy of the density of state close to the Fermi level (*11*), no difference between the two spectra is found, which points to the origin of the observed differences in the spectra lying elsewhere. Turning to the difference spectrum shown in Figure 2 as blue dotted line offset on the intensity axis, the shape in general agrees quite well with that of an O_2 gas O-K-edge

absorption spectrum (*14,15*). This means that any changes observed in the O-K-edge spectra with oxygen pressure are misleading, as they are originating from attenuation of the incident photon beam by the oxygen gas. What further complicates the issue is that beyond the strong resonances, the edge rise itself is pressure dependent. Any post-edge normalization of oxygen K-edges being exposed to different oxygen partial pressures is thus non-trivial.

To an extreme extent, the issue of the gas phase contribution had been identified before by Knop-Gericke et al. by using an elaborate sample setup with two detectors, one close to the sample, and one further away (*16*). In this case, the O_2 gas contributions were dominating in both recorded spectra, and the difference yielded a clean sample spectrum of the oxidized copper surface, as shown in Figure 3.

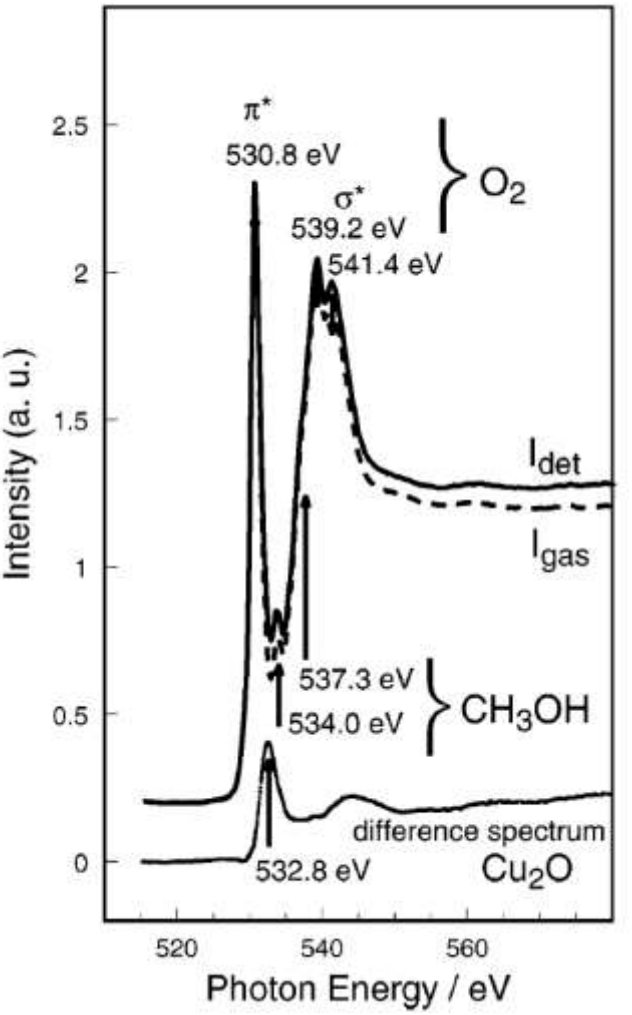

Figure 3. Oxygen K-edge spectra of 0.52 mbar of methanol on polycrystalline Cu taken in total electron yield. Reproduced with permission from Ref 16. Copyright 2000 Springer Nature.

Attenuation of Electrons: Influence of Detection Modes

It is important to distinguish the different modes and geometries of electron detection, which diverge in their manifestation of the signal attenuation phenomena. For a discussion of the general principles and a more in-depth discussion regarding the physics behind the processes, the reader is referred to the literature (*9*,*14*), but we will give a short account to illustrate the differences, as summarized in Figure 4.

In general, it is possible to either detect all electrons indiscriminately, or to select a certain range of kinetic energies to filter by. The former is consequently termed **total electron yield** (TEY), the latter **partial electron yield** (PEY). A special case of PEY is the Auger electron yield (AEY), where a specific Auger transition is used as a probe.

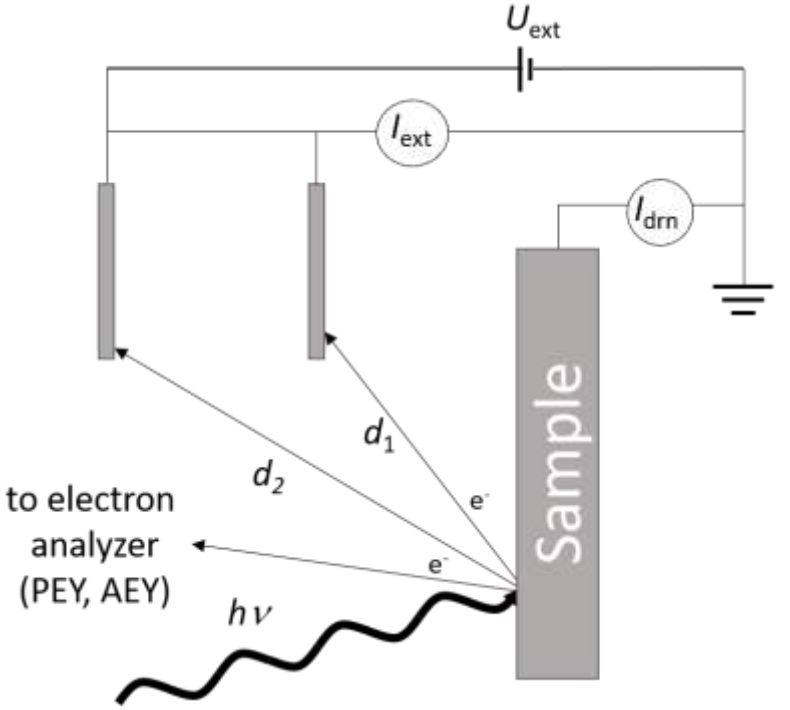

Figure 4. Schematic representation of the electron yield detection modes in XAS. Total Electron Yield (TEY) can either be collected by measuring the drain current I_{drn} directly from sample to ground, or by the current of electrons on a dedicated detector, extracted by an extraction voltage U_{ext}. If the extraction voltage is negative, it acts as a retarding filter to yield (partial electron yield, PEY). If electrons are extracted to an electron analyzer, a distinct window of kinetic energies detected can be chosen, allowing Auger electron yield (AEY) mode (see text for details).

Total Electron Yield

TEY can be further distinguished by the geometry of detection, as shown in Figure 4. Measuring the drain current I_{drn} directly on the sample accounts for all electrons leaving the sample through the photoexcitation event, as these are replenished by an external source. The I_{drn} is directly proportional to the absorption signal. Detecting the current of the electrons extracted from the surface (by applying an extraction voltage U_{ext}) I_{ext} would ideally yield an identical signal, provided the extraction is complete. Here, however, the electrons detected have to travel through the gas phase. Consequently, the signal will be attenuated, the magnitude being dependent on the path length and medium. This in turn presents an opportunity to correct for the gas phase attenuation of the electron yield signal by either using a reference sample at different pressures (being inert towards the gas medium), or by changing the distance *d* between the extractor and sample (as schematically shown in Figure 4). The TEY signal is dominated by a cascade of low-energy secondary electrons (< 40 eV) and is much more bulk sensitive than PEY (*17*).

Partial Electron Yield

In the PEY mode, a certain window of kinetic energies of electrons that are allowed to be passed to the detector is selected. This can be either done by applying a retarding voltage (acting as a high-pass filter) to the extraction electrode (U_{ext} being negative in Figure 4), or by using an electron analyzer, such as ones employed in photoelectron spectroscopy. The electron analyzer offers the freedom to use a specific type of signal. A prime example is the Auger electron yield mode (AEY), where a distinct Auger transition is selected and only electrons with the corresponding kinetic energy are accepted. Since in AEY the elastic Auger electrons dominate the yield signal, this mode provides the highest surface sensitivity, which is defined by their IMFP (*18*).

In multicomponent systems, the choice of kinetic energy windows can be quite limited as it needs to be made so that no photoemission peaks are shifting through the XAS, as illustrated in Figure 5. Using The $Sr(Ti,Co)O_3$ compound from Figure 2 as an example, collecting Co-L-edge XAS at photon energies between 770 and 800 eV, the O-KLL Auger transition cannot be used as the yield signal. Depending on the photon energy, the $Sr3d_{5/2}$ and $Sr3d_{3/2}$ photoemission peaks may contribute to the signal, which would result in artificial features in the XAS. In general, it is thus advisable to either use Auger transitions where no direct photoemission contribution is found for the whole incident photon energy range (which may be impossible, depending on compound), or to use a kinetic energy range where only the secondary background is present.

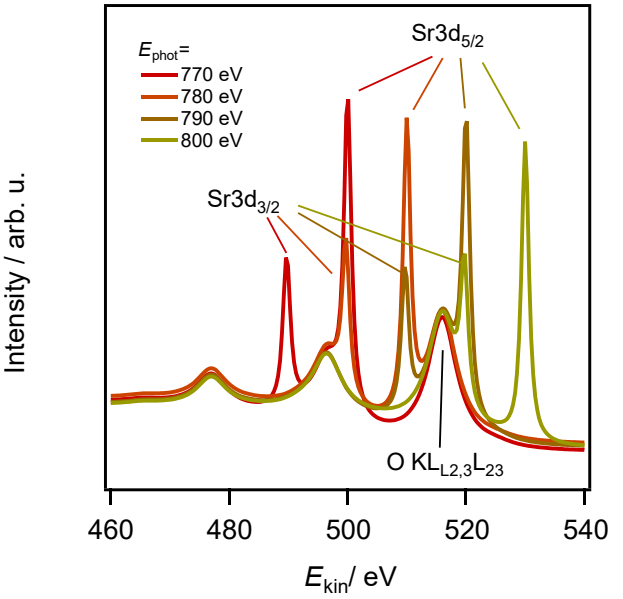

Figure 5: Simulated photoelectron spectra on $SrTi_{0.5}Co_{0.5}O_3$ for different incident photon energies. The O K-$L_{2,3}L_{2,3}$ line with constant kinetic energy is overlapped by Sr3d core level XPS (with constant binding energy) that shifts through the spectrum with photon energy.

In addition to the pure absorption effect (i.e., modulation of the incident beam intensity I_0 through the absorption edges of the solid), depending on the detection mode, a spectrum of the gas phase is also created and superimposed on the spectrum of the solid. The origin of the different electron yields is schematically shown in Figure 6, where electrons marked in red are from the gas phase and would yield a typical O_2 gas XAS at the oxygen K-edge. This is illustrated in Figure 7, which shows an O-K-edge spectrum on a polished gold foil in 1 Torr of O_2. Since no oxygen is present in the solid, no contribution from the solid is found and the spectrum exhibits the general shape of gas phase O_2 (ref. Figs 2 and 3). Consequently, if it is made sure that the distance between the sample and analyzer stays identical the spectrum acquired from the gold foil can be used to correct for the gas phase absorption of a different sample. However, this is experimentally quite challenging.

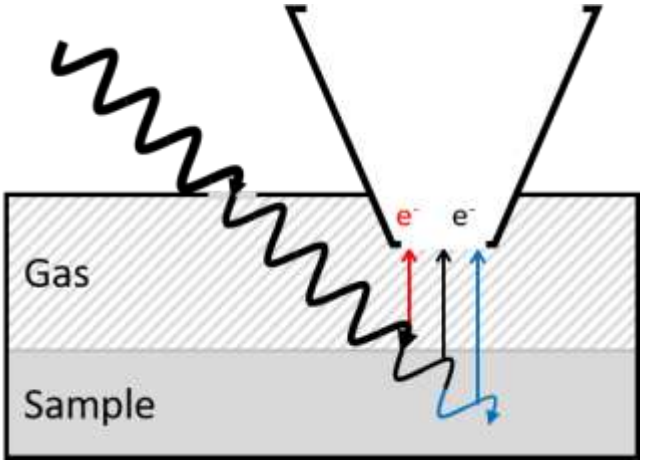

Figure 6. Schematic of an AP–XAS experiment in electron yield mode. The incident X-ray from the top left is attenuated by both the gas phase and the solid. The recorded spectrum at an absorption edge of an element common to both gas and solid will consist of contributions from the gas (red) and solid (black). Changing the acceptance window of emitted electrons to higher energies will add electrons originating from deeper inside the sample to the overall signal (blue), decreasing the fraction of electron from the gas phase. This is only true for electrons of KE > 100 eV.

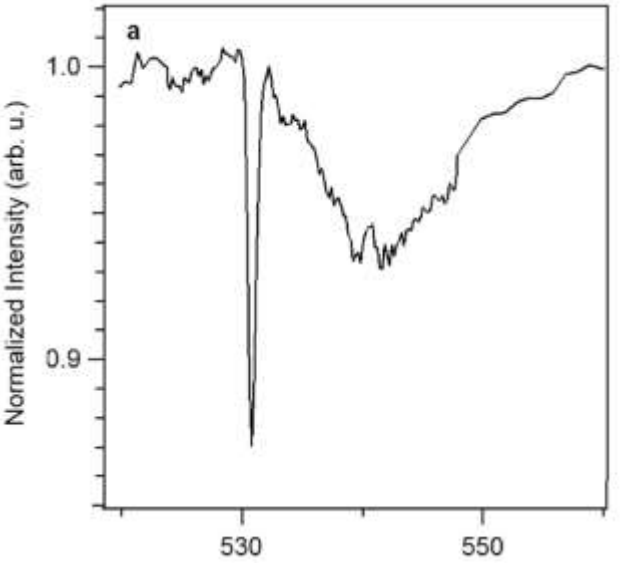

Figure 7. Oxygen K-edge collected at 500 °C at 1 Torr of oxygen on a polished Au foil. Reproduced with permission from Ref 11. Copyright 2015 Springer Nature.

11.

For a sample where oxygen is present in the solid, the contribution of the gas phase poses a problem, as it is superimposed on the oxygen XAS origination from the sample. How much the gas phase signal contributes to the total XAS depends on the kinetic energy window chosen for detection, as this determines the information depth, increasing the fraction of solid vs. gas phase that is accessed: If the volume of the solid sample contributing to the electron yield signal is decreased by increased surface sensitivity (through choosing a lower KE detection window), the fraction of the gas phase (its accessed volume being constant) becomes larger, as illustrated schematically in Figure 6 (electrons marked blue).

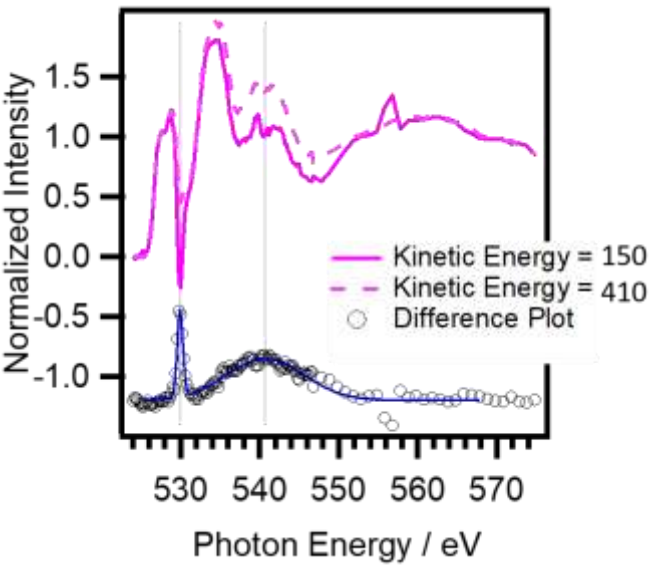

Figure 8. Oxygen K-edge spectra of (La,Sr)$FeO_{3-\delta}$ recorded at 500 °C in 1 Torr of O_2 in partial electron yield mode. The acceptance window was changed from 150 ± 5 eV (solid line) to 410 ± 5 eV (dashed line). The difference (open black circles) resembles the absorption of O_2 gas (blue line).

Experimentally, the above-described effect is shown in Figure 8 with data recorded at beamline 11.0.2. at the advanced light source (ALS), Berkeley. Here, the O-K-edge of (La,Sr)$FeO_{3-\delta}$ was collected at 500 °C in 1 Torr of oxygen, with the centers of acceptance window of the electrons collected for the partial electron yield signal being 150 and 410 eV (solid and dashed lines, respectively). Using the corresponding IMFP of electrons in the solid of 0.61 and 1.06 nm, respectively (*19*), it shows that roughly half the volume of the material is accessed in the more surface sensitive mode compared with the higher kinetic energy. With the distance between the sample surface and the analyzer cone of a typical AP–XPS/XAS setup (equaling the volume of the gas contributing to the signal, see electrons marked red in Figure 6) being tens to hundreds of µm (*20*), the volume fraction of signal-contributing gas phase vs. solid is 10^5 to 10^6, which coincidentally is roughly the factor between the density of the gas at typical AP–XAS pressures (up to 10 mbar) and the solid. This in turn means that depth profiling of the O-K-edge by variation of kinetic energy of collected electrons will introduce secondary effects by the gas phase, which will be challenging to deconvolute. Additionally, this means that comparing samples of different

composition where the kinetic energy windows need to be chosen differently to avoid overlapping with Auger transitions might become difficult.

To summarize, electron yield mode XAS experiments on samples that contain the same element(s) as the gas phase used to drive changes in the solid need to be either designed carefully with respect to possible contributions to the spectrum from the gas phase, or ways to minimize gas phase contributions need to be found. One way to do this would be to change the detection mode to fluorescence yield. However, this comes with its own problems, most prominently the loss of surface sensitivity, which is usually a crucial requirement for the relevant science. Another way to alleviate the issues is to find ways to drive reactions of the solid without changing the gas phase itself, i.e. electrochemically.

Eliminating Variation of Gas Phase Contributions

One way to drive redox reactions in oxides without changing the gas phase is through electrochemical means, which is limited to mixed ionic electronic conducting oxides and bears its own experimental challenges. For this purpose, the material to be investigated is made to be a part of an electrochemical cell, as shown schematically in Figure 9.

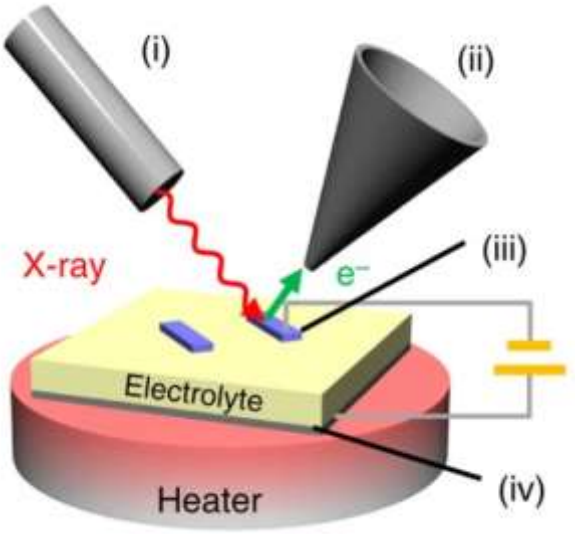

Figure 9. Artistic rendition of a solid state electrochemical. (i) incident X-rays, (ii) analyzer nozzle of the electron detector, (iii) working electrode, (iv) counter electrode. The electrochemical cell can be driven by applying a DC bias (orange), driving electrochemical reactions at the surface of the working electrode (blue). Reproduced with permission from Ref 11. Copyright 2015 Springer Nature.

When using an oxygen anion conducting electrolyte in an oxygen atmosphere, for example, Nernst's equation (3) can be formulated to describe an equivalency of applied electrical bias E in a gas atmosphere of partial pressure $p\mathrm{O}_2^{\mathrm{gas}}$ to an effective partial pressure $p\mathrm{O}_2^{\mathrm{eff}}$:

$$p\mathrm{O}_2{}^{\mathrm{eff}} = \exp\left(\frac{EnF}{RT}\right)^2 p\mathrm{O}_2{}^{\mathrm{gas}} \quad (3)$$

with *n* the number of electrons transferred in eq. (2), *F* the Faraday constant, *R* the gas constant, and *T* being the temperature. This leads to the generalized equivalence of chemical ($\Delta\mu_{O_2}$) and electrical potential *E* as elegantly and elaborately derived by Nenning et al. (*21*):

$$E = \frac{\Delta\mu_{O_2}}{4F} \quad (4)$$

The validity of this approach can (and should be) checked by several independent means, for example tracking of the electrostatic XPS binding energy shifts of inert electrolyte components (*11*,*22*) or impedance spectroscopy, deconvoluting potential drops across the different materials such as ohmic resistance of the electrolyte (*23*). Spectroscopically, this eliminates any differential contribution of the gas phase, as the (partial) pressure is kept constant throughout the experiments, and any observed changes in the spectra can then be attributed to the material itself. Though not explicitly stated, this might be the reason why many studies use electrochemical biasing instead of changing partial pressures through gas (mixtures). In the case of (La,Sr)$FeO_{3-\delta}$ (LSF), O-K-edge spectra at different biases driving the electrochemical reaction in a constant oxygen pressure of 1 Torr showed significant changes in the O-K-edge pre peaks attributed to the electronic states close to the Fermi level (*11*). Figure 10 shows the two different states and the correction by multiplying the spectra with the gas phase spectrum shown in Figure 7. This correction takes into account the diminishing of I_0.

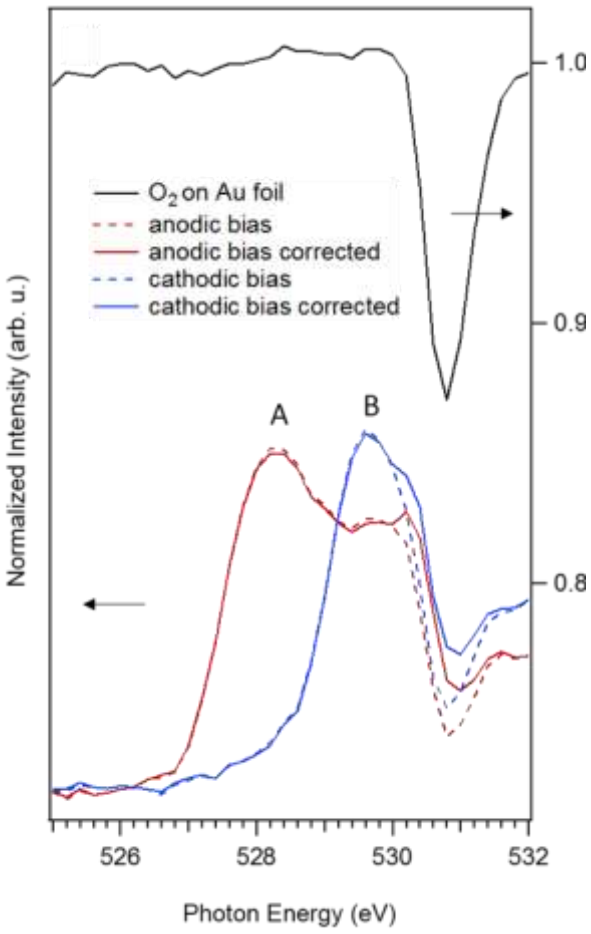

Figure 10. O-K-edge of an (La,Sr)$FeO_{3-\delta}$ cathode at 500 °C in 1 Torr of O_2 at different biases. The dashed lines are the same spectra corrected for the gas phase contribution collected on an Au foil. Reproduced with permission from Ref 11. Copyright 2015 Springer Nature.

Transmission XAS – Using Hard X-rays

Many of the experimental challenges in soft XAS have their root in the low penetration depths of photons (and electrons) at these energies, even in gaseous media of (below) atmospheric pressure. The switch to hard X-rays seems a natural workaround to alleviate these issues, and by choosing (much) higher energies and with that larger attenuation lengths, transmission XAS as a detection mode becomes viable.

The most immediate way of collecting an absorption spectrum would be in a transmission geometry, sending the incident photon beam through the sample and detecting the intensity before (I_0) and after the sample (I). The absorption spectrum would be given through Lambert Beer's Law:

$$I = I_0 e^{-\mu(E)d} \quad (5)$$

with μ(E) the absorption coefficient and d the thickness of the sample. To get meaningful spectra from this, naturally, the incident X-rays need to be able to penetrate the sample at least to a certain degree in order to have a sufficient intensity in the transmission signal. Figure 11 shows the absorption length of photons in Fe_3O_4 (red solid line). It can be clearly seen that in the soft XAS regime, sample thicknesses would have to be on the order of hundreds (or tens) of nanometers to achieve reasonable X-ray transmission. This stringent requirement becomes unrealistic when translated into the need for a free-standing thin film (with the same properties as the bulk material of interest) integrated into an *in situ* setup including high temperatures and pressures.

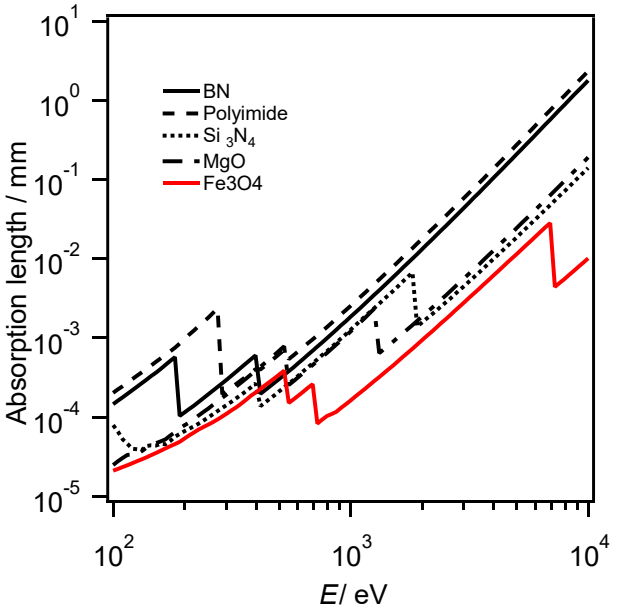

Figure 11. Photon absorption lengths of various materials used in in situ hard XAS experiments as well as Fe_3O_4 for comparison. Calculated using data from ref 3.

If the photon energies of the transitions of interest are high enough (>> 10 keV), however, any challenges pertaining to the presence of a reaction medium effectively vanish and become one of standard reactor design. For hard XAS studies on catalyst materials where noble metals are the active (and hence observed) species, a large number of works exist discussing the different experimental designs and are summarized elsewhere (*23*,*24*). At the photon energies of the 3d transition metal K-Edges, however, attenuation lengths in different media (including the gas phase) become of concern again. At the Fe-K-edge, our hypothetical Fe_3O_4 sample would have to be thinned to several µm thickness. Though this

has been done before (*25)*, diffusion limitation of the reaction and other mechanical issues might make the use of powder samples more feasible.

One standard strategy for using powder samples in hard X-ray spectroscopy is the dilution of the sample material with a less strongly absorbing one. The choice dilution materials here are of low *Z* and low density. Organic polymers are usually a good option in ex situ experiments. Unfortunately, for in situ or operando experiments, the selection of materials is limited to inert ones, not reacting with any gas atmosphere that might be present. This prevents polymers from being used, especially at elevated temperatures. Figure 11 shows the attenuation lengths of various standard dilution materials in our hypothetical case of Fe_3O_4 as the sample of interest. In an example experiment, tracking the oxidation of Fe_3O_4 at elevated temperatures through the Fe-K-edge (7.1 keV), BN, for example, shows an absorption length 30 times higher than that of the Fe_3O_4 and thus would be a suitable candidate. With this strategy, the chemical oxidation and reduction of Fe and Co in (Ba.Sr)(Fe,Co)$O_{3-\delta}$ was observed in situ (*26*). Here, the temperature, however, had to be limited to <600 °C to prevent a reaction with the BN. Previous attempts to exchange BN with MgO as a more resilient dilutant failed: At the Fe-K-edge, attenuation length of MgO is 20 µm, and with the experiment carried out at a bending magnet beamline (E4, DESY, Hamburg), the intensity was too low to yield acceptable data quality. With beamlines capable of delivering extremely high photon fluxes, a more lavish use of absorbent material for construction of experimental cells can be adopted. Eggart et al., for example, designed a cell where the photon beam crosses a reactor tube made of quartz glass, and spectra could be collected on a 0.5 wt% Fe loaded SiO_2 catalyst bed (*27*).

Information Obtained from Hard and Soft AP-XAS: Interpretation of Data

The first important difference in data obtained from both regimes is the information depth. While soft XAS is (also by virtue of the detection mode) quite surface sensitive, hard XAS will access the bulk. The vast majority of the materials studied using the ambient pressure variants of the two techniques, however, undergo changes of the surface electronic structure and chemistry (hence those materials are interesting to study *in situ* in the first place) when exposed to reactive gas atmospheres and/or elevated temperatures. Mixed conducting oxides, for example, show a tendency to accumulate charged point defects at the very surface (*28*), making bulk studies incapable of elucidating the underlying mechanisms. Another effect that changes surface properties is the buildup of surface space charge layers that are oxygen partial pressure dependent (*29*), which occurs at temperatures where any bulk defect chemistry is still frozen. Lastly, aliovalent co-substituted compounds, such as ABO_3 perovskite oxides, can suffer from cationic segregation and precipitation reactions, rendering (defect) chemistry and electronic structure considerably different from that of the bulk (*30*). It is thus important to choose the X-ray regime according to the information one wants to gather. Equally important is the use of other techniques (spectroscopic or other) to verify interpretations, especially when it comes to using (physico-)chemical formalisms, such as “ionic charge” and “oxidation state”.

To exemplify this, we understand that Fermi’s golden rule dictates that the allowed dipole transitions are limited to $\Delta l = \pm 1$ and $\Delta m_l = 0, \pm 1$, with l and m_l the azimuthal and magnetic quantum numbers, respectively (*31*). This means that, depending on the material, transitions can either occur into localized states or, if no states of the “correct” symmetry are empty, into the vacuum. Let’s apply the rule to the ubiquitous case of 3d transition

metal oxides. In the soft X-ray regime, the unoccupied oxygen states are accessible through the 1s to 2p transition. This is only possible because all transition metal oxides show a certain degree of hybridization and negative charge transfer between the O2p and TM3d states (*32*-*34*). Otherwise, in a hypothetical O^{2-} anion embedded in a solid lattice with the electron configuration $1s^2 2s^2 p^6$, no unoccupied p states would exist. This discrepancy to the usual formalism of solid-state electrochemistry, where the O^{2-} entity unequivocally exists (*35*), already shows that soft XAS is only conditionally useful to determine such quantities as "oxidation state" and "ionic charge".

Complementary to the oxygen in the charge scheme of the oxides are the transition metal absorption edges. These also carry their share of ambiguities. The Fe-L-edges are, for example, routinely used to quantify the state of charge in a $LiFePO_4$ electrode material (*36*). However, this is in contrast with SOFC cathode materials, where both Fe- and Co-L-edges are silent upon electrochemical oxidation and reduction (*11*). Here, the hard X-ray pendants, the Fe- and Co-K-edges, might give more insight: Chemical oxidation and reduction in a transmission experiment, for example, could show edge shifts of the K-edges (*26*), usually interpreted as a change in oxidation states. Is this discrepancy between the TM-L- and K-edges now an effect of different probing depths? Most likely not, as edge shifts in the K-edge can also originate from structural changes in these types of materials (*37*,*38*). This, however, is universally true and not singular to the ambient pressure variants of XAS, and thus beyond the scope of this chapter.

Summary

The use of X-ray absorption spectroscopy in its ambient pressure variant is an important tool in the suite of *operando* techniques, especially to follow chemical processes in real time. We have discussed a thus far underrepresented aspect, the implications of having an atmosphere interact with the X-ray in addition to the sample itself. This becomes especially an issue when the atmosphere and solid sample share the same type of elements, which is–unfortunately–true for many experiments. Understanding these processes and strategies to either minimize these unwanted contributions to the spectra experimentally or filter them out in data analysis is of high importance, mostly, but not only, for soft X-ray absorption spectroscopy.

Acknowledgements

Helpful discussion and proof reading with/by Dr. Tomáš Duchoň and Dr. Stefan Cramm is gratefully acknowledged.

References

(1) Ogletree, F. D.; Bluhm, H.; Hebenstreit, E. D.; Salmeron, M. Photoelectron Spectroscopy under Ambient Pressure and Temperature Conditions. *Nucl. Instruments Methods Phys. Res. Sect. A Accel. Spectrometers, Detect. Assoc. Equip.* **2009**, 601, 151–160. https://doi.org/10.1016/j.nima.2008.12.155.

(2) M. P. Seah; W. A. Dench. *Quantitative Electron Spectroscopy of Surface. Surf. Interface Anal.* **1979**, 1, 2.

(3) Henke, B. L.; Gullikson, E. M.; Davis, J. C. X-ray Interactions: Photoabsorption, Scattering, Transmission, and Reflection at E = 50-30, 000 EV, Z = 1-92. *Atomic Data and Nuclear Data Tables*. **1993**, 181–342. https://doi.org/10.1006/adnd.1993.1013.

(4) Norby, T. A Kröger-Vink Compatible Notation for Defects in Inherently Defective Sublattices. *J. Korean Ceram. Soc.* **2010**, 47, 19–25. https://doi.org/10.4191/KCERS.2010.47.1.019.

(5) Merkle, R.; Maier, J. How Is Oxygen Incorporated into Oxides? A Comprehensive Kinetic Study of a Simple Solid-State Reaction with $SrTiO_3$ as a Model Material. *Angew. Chemie Int. Ed*. **2008**, 47, 3874–3894. https://doi.org/10.1002/anie.200700987.

(6) Richter, J.; Holtappels, P.; Graule, T.; Nakamura, T.; Gauckler, L. J. Materials Design for Perovskite SOFC Cathodes. *Monatshefte fur Chemie* **2009**, 140, 985–999. https://doi.org/10.1007/s00706-009-0153-3.

(7) Sunarso, J.; Baumann, S.; Serra, J. M.; Meulenberg, W. A.; Liu, S.; Lin, Y. S.; Diniz da Costa, J. C. Mixed Ionic-Electronic Conducting (MIEC) Ceramic-Based Membranes for Oxygen Separation. *J. Memb. Sci.* **2008**, 320, 13–41. https://doi.org/10.1016/j.memsci.2008.03.074.

(8) Suntivich, J.; Hong, W. Estimating Hybridization of Transition Metal and Oxygen States in Perovskites from OK-Edge X-ray Absorption Spectroscopy. *J. Phys. Chem. C* **2014**, 118, 1856–1863.

(9) de Groot, F. M. F.; Gironi, M.; Fuggle, J. C.; Ghijsen, J.; Sawatzky, A.; Petersen, H. Oxygen 1s X-ray-Absorption. *Phys. Rev. B* **1989**, 40, 5715–5723.

(10) Abbate, M.; de Groot, F. M. F.; Fuggle, J. C.; Strebel, O.; Lopez, F.; Domke, M.; Kaindl, G.; Sawatzky, G. A.; Takano, M.; Takeda, Y.; Eisaki, H.; Uchida, S. Controlled-Valence of $La_{1-x}Sr_xFeO_3$ and $La_{1-x}Sr_xMnO3$ Studied by Soft X-ray Absorption Spectroscopy. *Phys. Rev. B* **1992**, 46, 4511–4519. https://doi.org/10.1103/PhysRevB.46.4511.

(11) Mueller, D. N.; Machala, M. L.; Bluhm, H.; Chueh, W. C. Redox Activity of Surface Oxygen Anions in Oxygen-Deficient Perovskite Oxides during Electrochemical Reactions. *Nat. Commun.* **2015**, 6, 6097. https://doi.org/10.1038/ncomms7097.

(12) Frati, F.; Hunault, M. O. J. Y.; De Groot, F. M. F. Oxygen K-Edge X-ray Absorption Spectra. *Chem. Rev.* **2020**, 120, 4056–4110. https://doi.org/10.1021/acs.chemrev.9b00439.

(13) Liu, Y.; Baumann, S.; Schulze-Küppers, F.; Mueller, D. N.; Guillon, O. Co and Fe Co-Doping Influence on Functional Properties of $SrTiO_3$ for Use as Oxygen Transport Membranes. *J. Eur. Ceram. Soc.* **2018**, 38, 5058–5066. https://doi.org/10.1016/j.jeurceramsoc.2018.07.037.

(14) Stoehr, *J. NEXAFS Spectroscopy*, Corr. 2nd.; Springer-Verlag: Berlin, **2003**.

(15) Pan, G.; He, G.; Zhang, M.; Zhou, Q.; Tyliszczak, T.; Tai, R.; Guo, J.; Bi, L.; Wang, L.; Zhang, H. Nanobubbles at Hydrophilic Particle-Water Interfaces. *Langmuir* **2016**, 32, 11133–11137. https://doi.org/10.1021/acs.langmuir.6b01483.

(16) Knop-Gericke, A.; Hävecker, M.; Schedel-Niedrig, T.; Schlögl, R. High-Pressure Low-Energy XAS: A New Tool for Probing Reacting Surfaces of Heterogeneous Catalysts. *Top. Catal.* **2000**, 10, 187–198. https://doi.org/10.1023/A:1019101109313.

(17) Erbil, E.; Cargil, G. S.; Frahm, R.; Boehme, R. F. Total-electron-yield current measurements for near-surface extended x-ray-absorption fine structure, *Phys. Rev. B* **1988**, 37, 2450-2464. https://doi.org/10.1103/PhysRevB.37.2450.

(18) Schroeder, S. L. M.; Moggridge, G. D.; Ormerod, R. M.; Rayment, T.; Lambert, R. M. What determines the probing depth of electron yield XAS? *Surf. Sci.* **1995**, 324, L371-L377. https://doi.org/10.1016/0039-6028(94)00779-9.

(19) Tanuma, S.; Powell, C. J.; Penn, D. R. Calculations of Electron Inelastic Mean Free Paths. *Surf. Interface Anal.* **1994**, 21, 165–176.

(20) Zhu, S.; Scardamaglia, M.; Kundsen, J.; Sankari, R.; Tarawneh, H.; Temperton, R.; Pickworth, L.; Cavalca, F.; Wang, C.; Tissot, H.; Weissenrieder, J.; Hagman, B.; Gustafson, J.; Kaya, S.; Lindgren, F.; Kallquist, I.; Maibach, J.; Hahlin, M.; Boix, V.; Gallo, T.; Rehman, F.; D'Acunto, G.; Schnadta, J.; Shavorskiy, A. HIPPIE: A New Platform for Ambient-Pressure X-ray Photoelectron Spectroscopy at the MAX IV Laboratory. *J. Synchrotron Radiat.* **2021**, 28, 624–636. https://doi.org/10.1107/S160057752100103X.

(21) Nenning, A.; Opitz, A.; Rameshan, C.; Rameshan, R.; Blume, R.; Hävecker, M.; Knop-Gericke, A.; Rupprechter, G.; Klötzer, B.; Fleig, J. Ambient Pressure XPS Study of Mixed Conducting Perovskite-Type SOFC Cathode and Anode Materials under Well-Defined Electrochemical Polarization. *J. Phys. Chem. C* **2016**, 120, 1461–1471. https://doi.org/10.1021/acs.jpcc.5b08596.

(22) El Gabaly, F.; Grass, M.; McDaniel, A. H.; Farrow, R. L.; Linne, M. A.; Hussain, Z.; Bluhm, H.; Liu, Z.; McCarty, K. F. Measuring Individual Overpotentials in an Operating Solid-Oxide Electrochemical Cell. *Phys. Chem. Chem. Phys.* **2010**, 12, 12138–12145. https://doi.org/10.1039/c003581e.

(23) Nenning, A.; Fleig, J. Electrochemical XPS Investigation of Metal Exsolution on SOFC Electrodes: Controlling the Electrode Oxygen Partial Pressure in Ultra-High-Vacuum. *Surf. Sci.* **2019**, 680, 43–51. https://doi.org/10.1016/j.susc.2018.10.006.

(23) Grunwaldt, J. D.; Caravati, M.; Hannemann, S.; Baiker, A. X-ray Absorption Spectroscopy under Reaction Conditions: Suitability of Different Reaction Cells for Combined Catalyst Characterization and Time-Resolved Studies. *Phys. Chem. Chem. Phys.* **2004**, 6, 3037–3047. https://doi.org/10.1039/b403071k.

(24) Doronkin, D. E.; Lichtenberg, H.; Grunwaldt, J. XAFS Techniques for Catalysts, Nanomaterials, and Surfaces. *XAFS Tech. Catal. Nanomater. Surfaces* **2017**. https://doi.org/10.1007/978-3-319-43866-5.

(25) Hilbrandt, N.; Martin, M. DEXAFS — a New Technique to Investigate the Kinetics of High Temperature Solid State Reactions in Situ. *Solid State Ionics* **1997**, 95, 61–64.

(26) Mueller, D. N.; De Souza, R. A.; Brendt, J.; Samuelis, D.; Martin, M. Oxidation States of the Transition Metal Cations in the Highly Nonstoichiometric Perovskite-Type Oxide $Ba_{0.1}Sr_{0.9}Co_{0.8}Fe_{0.2}O_{3-\delta}$. *J. Mater. Chem.* **2009**, 19, 1960. https://doi.org/10.1039/b819415g.

(27) Eggart, D.; Zimina, A.; Cavusoglu, G.; Casapu, M.; Doronkin, D. E.; Lomachenko, K. A.; Grunwaldt, J. D. Versatile and High Temperature Spectroscopic Cell for Operando Fluorescence and Transmission X-ray Absorption Spectroscopic Studies of Heterogeneous Catalysts. *Rev. Sci. Instrum.* **2021**, 92, 023106. https://doi.org/10.1063/5.0038428.

(28) Chueh, W. C.; Mcdaniel, A. H.; Grass, M. E.; Hao, Y.; Jabeen, N.; Liu, Z.; Haile, S. M.; Mccarty, K. F.; Bluhm, H.; Gabaly, F. El. Highly Enhanced

Concentration and Stability of Reactive Ce^{3+} on Doped CeO_2 Surface Revealed In Operando. *Chem. Mater.* **2012**, 24, 1876–1882.

(29) Andrä, M.; Dvořák, F.; Vorokhta, M.; Nemšák, S.; Matolín, V.; Schneider, C. M.; Dittmann, R.; Gunkel, F.; Mueller, D. N.; Waser, R. Oxygen Partial Pressure Dependence of Surface Space Charge Formation in Donor-Doped $SrTiO_3$. *APL Mater.* **2017**, 5. 056106. https://doi.org/10.1063/1.4983618.

(30) Lee, W.; Han, J. W.; Chen, Y.; Cai, Z.; Yildiz, B. Cation Size Mismatch and Charge Interactions Drive Dopant Segregation at the Surfaces of Manganite Perovskites. *J. Am. Chem. Soc.* **2013**, 135, 7909–7925. https://doi.org/10.1021/ja3125349.

(31) Rehr, J. J. Theory and Calculations of X-ray Spectra: XAS, XES, XRS, and NRIXS. *Radiat. Phys. Chem.* **2006**, 75, 1547–1558. https://doi.org/10.1016/j.radphyschem.2005.11.014.

(32) de Groot, F. M. F. X-ray Absorption of Transition Metal Oxides: An Overview of the Theoretical Approaches. *J. Electron Spectros. Relat. Phenomena* **1993**, 62, 111–130. https://doi.org/10.1016/0368-2048(93)80009-B.

(33) Chen, J. G. NEXAFS Investigations of Transition Metal Oxides, Nitrides, Carbides, Sulfides and Other Interstitial Compounds. *Surf. Sci. Rep.* **1997**, 30, 1–152. https://doi.org/10.1002/chin.199819267.

(34) Bocquet, A. E.; Mizokawa, T.; Morikawa, K.; Fujimori, A.; Barman, S. R.; Maiti, K.; Sarma, D. D.; Tokura, Y.; Onoda, M. Electronic Structure of Early 3 d -Transition-Metal Oxides by Analysis of the 2 p Core-Level Photoemission Spectra. *Phys. Rev. B* **1996**, 53, 1161–1170. https://doi.org/10.1103/PhysRevB.53.1161.

(35) De Souza, R. A.; Mueller, D. N. Electrochemical Methods for Determining Ionic Charge in Solids. *Nat. Mater.* **2021**, 20, 443–446. https://doi.org/10.1038/s41563-020-0790-9.

(36) Li, Y.; El Gabaly, F.; Ferguson, T. R.; Smith, R. B.; Bartelt, N. C.; Sugar, J. D.; Fenton, K. R.; Cogswell, D. A.; Kilcoyne, A. L. D.; Tyliszczak, T.; Bazant, M. Z.; Chueh, W. C. Current-Induced Transition from Particle-by-Particle to Concurrent Intercalation in Phase-Separating Battery Electrodes. *Nat. Mater.* **2014**, 13, 1149–1156. https://doi.org/10.1038/nmat4084.

(37) Orikasa, Y.; Crumlin, E. J.; Sako, S.; Amezawa, K.; Uruga, T.; Biegalski, M. D.; Christen, H. M.; Uchimoto, Y.; Yang, S. H. Surface Strontium Segregation of Solid Oxide Fuel Cell Cathodes Proved by in Situ Depth-Resolved X-ray Absorption Spectroscopy. *ECS Electrochem. Lett.* **2014**, 3. https://doi.org/10.1149/2.006404eel.

(38) Heuer, S. A.; Schierholz, R.; Alekseev, E. V.; Peters, L.; Mueller, D. N.; Duchoň, T.; Vibhu, V.; Tempel, H.; De Haart, L. G. J.; Kungl, H.; Eichel, R. A. Oxygen Nonstoichiometry and Valence State of Manganese in $La_{1-x}Ca_xMnO_{3+\delta}$. *ACS Omega* **2021**, 6, 9638–9652. https://doi.org/10.1021/acsomega.1c00208.